Korean J. Chem. Eng., 35(9), 1815-1822 (2018)
DOI: 10.1007/s11814-018-0090-0

pISSN: 0256-1115
eISSN: 1975-7220

Methane combustion over Pd/Ni-Al oxide catalysts: Effect of Ni/Al ratio in the Ni-Al oxide support

Eunpyo Hong*, Su-A Jeon*, Sang-Sup Lee, and Chae-Ho Shin*,†**

*Department of Chemical Engineering, Chungbuk National University, Chungbuk 28644, Korea
**Department of Environmental Engineering, Chungbuk National University, Chungbuk 28644, Korea
(*Received 8 April 2018 • accepted 27 May 2018*)

Abstract−We prepared xNi-2Al oxide (x=0-1.1) supports via a hydrothermal method, and applied Pd/xNi-2Al catalysts in the catalytic methane combustion reaction. It was found that the physicochemical properties of the xNi-2Al supports varied as a function of the Ni content, and the interaction between support and impregnated Pd was also influenced by the Ni content. Furthermore, variation in the Ni content significantly affected the chemical state and reducibility of the impregnated Pd species. Finally, the catalytic activity and stability of prepared Pd/xNi-2Al catalysts in the methane combustion reaction exhibited a volcano-shaped curve as a function of Ni content, with a maximum being observed for the Pd/1.0Ni-2Al catalyst, which corresponded to the highest Pd^{2+} composition and reducibility.

Keywords: Ni-Al Oxide, Palladium, Methane Combustion, Hydrothermal Method, Deactivation

INTRODUCTION

Global warming caused by the release of greenhouse gases is currently receiving significant amounts of research interest [1], suggesting that the removal of methane from gaseous emissions is of particular importance, as methane is the second largest contributor (~19%) to global warming after carbon dioxide (~64%). Although the combustion of methane produces carbon dioxide, it is an effective way to reduce the global warming potential, as methane exhibits a greenhouse potential approximately 21 times greater than that of carbon dioxide [2]. However, conventional thermal combustion methods require the use of extremely high temperatures (~1,600 °C), which also result in the production of both thermal NO_x and CO. In contrast, catalytic methane combustion can remove methane containing low concentrations of thermal NO_x at relatively low temperatures (<500 °C) [3-7], and so it has received growing attention for use in various industrial facilities, such as natural gas-fueled engines, boilers and incinerators for energy production, and exhaust gas control [8].

Supported noble metal catalysts, such as Pt, Au, Rh, and Pd, have been extensively studied in methane combustion, with supported Pd catalysts being the most effective [9-12]. Thus, the relationships between catalytic activity, Pd dispersion (particle size), active Pd species, and metal-support interactions have received significant attention. For example, the chemical state of the active Pd species is known to have a particular influence on catalytic activity in the methane combustion reaction. Although Pd can be present in the form of Pd^0, Pd^{2+}, and Pd^{4+}, the Pd^{2+} originating from PdO is generally accepted as the active species for combustion reaction [3,4]. Although Pd^0 and Pd^{4+} are mostly considered inactive, a number of studies have suggested that Pd^0 is involved in the adsorption and activation of methane [13,14]. In addition, interactions between the Pd species and the support play a major role in the formation and preservation of the Pd^0, Pd^{2+}, and Pd^{4+} species [4,15].

To date, the application of various supports, including Al_2O_3 [4, 11,15,16], CeO_2 [17], SnO_2 [18,19], SiO_2 [20], and ZrO_2 [3,10] has been investigated for the combustion reaction. Although spinel-structured supports [13,21-23] such as $MgAl_2O_4$, $CoAl_2O_4$, and $NiAl_2O_4$ also exhibit potential due to their high thermal stabilities, the application of such supports has been limited due to their relatively low specific surface areas compared to the commonly used Al_2O_3 support. Until now, $NiAl_2O_4$ has been mainly employed as a promoter to modify the interface between the support and the active metal species [24-26].

In addition to successful methane conversion, the stability during the catalytic reaction is also a critical factor for practical applications. In the case of supported Pd catalysts, the stability is largely influenced by the presence of water, which usually acts as an inhibitor to form the inactive $Pd(OH)_2$ species during the reaction [11, 27,28]. It is therefore of particular importance to examine the hydrothermal stability, as water is normally present in the reaction feed, in addition to being produced during the combustion reaction itself.

Thus, we employed a hydrothermal method for the preparation of Ni-Al oxide supports containing different Ni/Al ratios. Subsequently, 0.5 wt% Pd/Ni-Al oxide catalysts were applied to methane combustion experiments. To examine the hydrothermal stability of catalysts in the methane combustion reaction, comparative experiments were carried out in the presence and absence of 3% water vapor. To characterize the synthesized catalysts and to determine the relationship between the catalyst characteristics and the catalytic performance (conversion and hydrothermal stability), N_2-sorption, X-ray diffraction (XRD), *iso*-propanol temperature-programmed desorption (IPA-TPD), X-ray photoelectron spectroscopy (XPS), and CH_4 temperature-programmed reduction (CH_4-TPR) analy-

†To whom correspondence should be addressed.
E-mail: chshin@chungbuk.ac.kr

ses were conducted.

EXPERIMENTAL

1. Catalyst Preparation

The Al_2O_3 and Ni-Al oxide supports were synthesized via a hydrothermal method using $Ni(NO_3)_2 \cdot 6H_2O$ (98%, Samchun) and $Al(NO_3)_3 \cdot 9H_2O$ (99%, Junsei) as precursors. After dissolving both precursors in deionized water, a 2 M aqueous solution of NaOH (prepared from NaOH powder, 99%, Jinchemical) was added dropwise to the precursor solution until the pH reached 9.5. The resulting solution was then stirred at 25 °C for 0.5 h, after which time it was hydrothermally treated at 150 °C for 5 h in an autoclave, and the obtained solid precipitate was filtered and washed exhaustively with deionized water. Finally, the precipitate was dried at 100 °C for 24 h and the dried product was calcined at 900 °C for 2 h. In this study, xNi-2Al supports were prepared, where x represents the 2Ni/Al molar ratio (x=0-1.1). The 0.5 wt% Pd/xNi-2Al catalysts were then synthesized via an incipient wetness method using a $Pd(NO_3)_2$ solution (10 wt%, Heesung Catalysts Corp.). All catalysts were dried at 100 °C for 24 h prior to calcination at 600 °C for 2 h under a flow of air (1,000 cm^3/min).

2. Characterization

To estimate the textural properties (i.e., specific surface area, total pore volume, and average pore size) of the obtained products, N_2-sorption isotherms were carried out using a ASAP 2020 (Micromeritics). Prior to N_2-sorption analysis, the samples were degassed at 250 °C for 5 h under vacuum. To identify the crystalline structures of the xNi-2Al supports and the Pd/xNi-2Al catalysts, XRD was carried out using a D8 Discover with GADDS (Bruker AXS) X-ray diffractometer using Cu Kα radiation, with 40 kV accelerating voltage and 40 mA applied current. From the XRD patterns, the crystal size (D, nm) was calculated using the Scherrer equation (Eq. (1)):

$$D = k\lambda/\beta\cos\theta \quad (1)$$

where k is the shape factor of the particle (0.89), λ is the X-ray wavelength (0.15406 nm), β is the corrected full width at half maximum (FWHM) in radian, and θ is the Bragg diffraction angle in degrees.

All IPA-TPD measurements involved using a quadrupole mass spectrometer (GSD 301, Pfeiffer Vacuum). In each case, the sample (0.1 g) was loaded into a U-shaped quartz reactor using quartz wool and pretreated at 300 °C for 0.5 h under a stream of Ar. After cooling to room temperature, the sample was exposed to 3 kPa of IPA for 0.5 h, and then purged with Ar for 0.5 h to remove the physically adsorbed IPA. Subsequently, the temperature was elevated to 400 °C with a heating rate of 10 °C/min under a flow of Ar. During the IPA-TPD measurements, the total flow was fixed at 30 cm^3/min. The surface chemical states of the Pd species in the Pd/xNi-2Al catalysts were identified by XPS using an PHI Quantera-II (Ulvac-PHI) photoelectron spectrometer (Al Kα radiation; hν=1486.6 eV), and the XPS data were calibrated using the binding energy of adventitious carbon (i.e., C 1s, 284.6 eV) as a standard. To further interpret the XPS results, peak-fitting and deconvolution of the Pd 3d spectra were carried out using the Gaussian-Lorentzian curve-fitting method after background subtraction by the Shirley method, with constant FWHM value of 2 eV. To investigate the reduction characteristics of the supported PdO species, CH_4-TPR was performed. In each case, the sample (0.1 g) was loaded into a fixed bed quartz reactor, and the temperature was elevated to 900 °C with a heating rate of 10 °C/min under an environment of 1% CH_4/N_2 (total flow=50 cm^3/min) without pretreatment of the sample. The quantity of CH_4 consumed was analyzed using an infrared gas analyzer (Model 7500, Teledyne Analytical Instruments).

3. Methane Combustion Reaction

For the methane combustion reaction, the Pd/xNi-2Al catalysts (0.1 g) were loaded into a U-shaped quartz fixed bed reactor. Prior to the reaction, pretreatment was carried out under a stream of Air (100 cm^3/min) at 600 °C for 1 h. The reaction gas composition was then adjusted to 1% CH_4/20% O_2/N_2 balance and a total flow rate of 200 cm^3/min in the presence and absence of 3% water vapor. The temperature-programmed reaction proceeded from 200 to 600 °C with a heating rate of 4 °C/min, and the isothermal reaction was allowed to proceed at 370 °C for 20 h. The CH_4 concentration was measured using an infrared gas analyzer (Model 7500, Teledyne Analytical Instruments), and the CH_4 conversion was calculated using Eq. (2):

$$CH_4 \text{ conversion (X, \%)} = \frac{CH_{4\,in} - CH_{4\,out}}{CH_{4\,in}} \times 100 \quad (2)$$

where $CH_{4\,in}$ and $CH_{4\,out}$ are the concentrations of CH_4 at the inlet and outlet, respectively.

RESULTS AND DISCUSSION

1. N_2-sorption Analysis

The N_2-sorption isotherms of the xNi-2Al supports and the Pd/xNi-2Al catalysts are shown in Fig. S1, and their texture properties are summarized in Table 1. According to IUPAC classification, all isotherms can be categorized as type IV isotherms with a type H2 hysteresis loop, indicating that all supports and catalysts exhibited mesoporous structures. In addition, from the data shown in

Table 1. Specific surface areas (S_{BET}), total pore volumes (V_P), and average pore sizes (D_P) of the xNi-2Al supports and the Pd/xNi-2Al catalysts as determined from the N_2-sorption isotherms

x	xNi-2Al			Pd/xNi-2Al		
	S_{BET} (m^2/g)	V_P[a] (cm^3/g)	D_P[b] (nm)	S_{BET} (m^2/g)	V_P[a] (cm^3/g)	D_P[b] (nm)
0	136	0.370	8.6	134	0.380	8.5
0.8	96	0.300	9.2	87	0.281	9.7
0.9	76	0.291	11.1	70	0.272	11.5
1.0	74	0.279	11.4	71	0.275	12.0
1.1	70	0.267	11.7	64	0.253	12.2

[a]Obtained from the volume of N_2 adsorbed at P/P_0=0.995
[b]Calculated from the desorption branch of the N_2 isotherm using the Barrett-Joyner-Halenda method

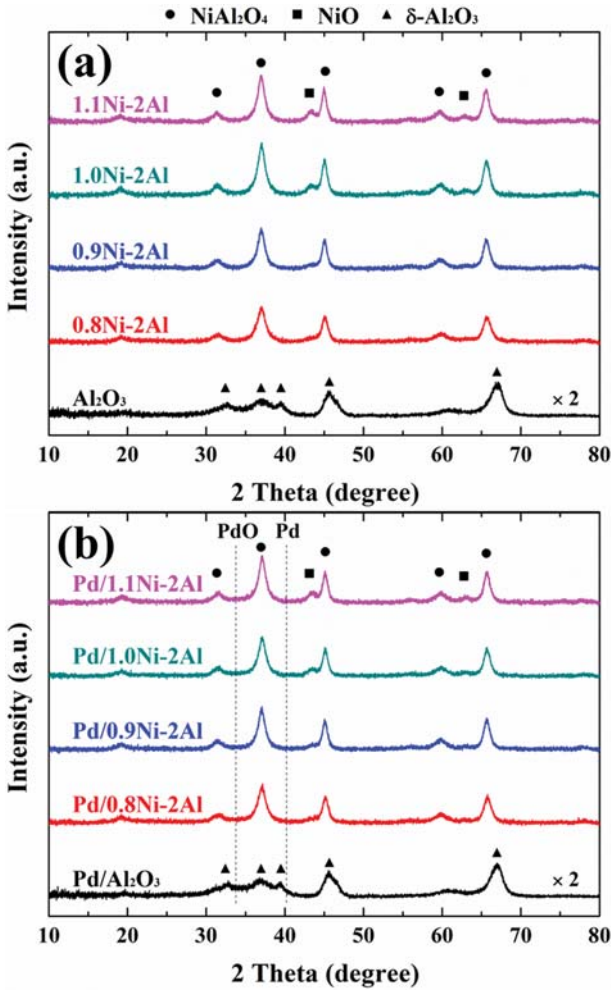

Fig. 1. XRD patterns of (a) the xNi-2Al supports and (b) the Pd/xNi-2Al catalysts.

Table 1, the specific surface areas of the xNi-2Al supports appeared to decrease gradually upon increasing the Ni content, likely due to a decrease in the total pore volume and an increase in the average pore size. This tendency was also observed for the Pd/xNi-2Al catalysts, and the slight decrease in specific surface area of these catalysts following Pd impregnation was due to partial blockage of the porous support structure by the impregnated Pd.

2. XRD and Surface Elemental Analyses

The XRD patterns of the xNi-2Al supports and the Pd/xNi-2Al catalysts are shown in Fig. 1. It is well known that the crystalline phase of Al_2O_3 can be changed depending on calcination temperature and precursor species [29-32]. In this case (see Fig. 1(a)), the use of an $Al(NO_3)_3 \cdot 9H_2O$ precursor and calcination at 900 °C for 2 h produced a crystalline δ-Al_2O_3 phase (JCPDS No. 16-0394). Although the spinel $NiAl_2O_4$ (JCPDS No. 10-0339) was the major crystalline phase in the samples of sub-stoichiometric compositions (i.e., 0.8Ni-2Al and 0.9Ni-2Al), a small shoulder peak of NiO (JCPDS No. 89-5881) at 2 theta value of 43.3° was also observed. In addition, this peak corresponding to NiO increased upon increasing the Ni content. This result well matched the surface atomic composition obtained by XPS analysis as summarized in Table 2. The surface atomic compositions of all samples exhibited lower Al/Ni ratios compared to theoretical atomic composition, thereby indicating that excess Ni species existed at the surface. From the literature [33], the co-precipitated nickel aluminate is not completely homogeneous, and so local composition of this mixed oxide is separated into Al-rich and Ni-rich regions. This phenomenon was also observed over calcined catalysts [34,35]. Therefore, the co-precipitated samples employed herein were initially formed as a partially separated form, and Ni-rich structure seems to migrate toward catalyst surface during the hydrothermal treatment at 150 °C for 5 h in an autoclave. In addition, for all catalysts examined, no obvious characteristic Pd and PdO signals were detected due to the low loading and high dispersity of the Pd species.

3. IPA-TPD Measurement

To investigate the surface characteristics of the xNi-2Al supports, the surface acidities were measured by means of IPA-TPD analysis. Since IPA molecules can react on different types of active sites to produce a range of products, IPA-TPD analysis could be one of the useful tools for determining the surface properties [36,37]. For example, the IPA dehydration pathway occurs on acidic sites to produce propylene ($\cdot C_3H_5$ fragment of the propylene radical, m/z= 41), which can be employed as a probe molecule to determine the surface acid characteristics [38]. As indicated by the IPA-TPD results for the xNi-2Al supports shown in Fig. 2, the relative peak areas of the produced propylene gradually decreased as the Ni content was increased, thereby suggesting that the number of acidic sites on

Table 2. Physicochemical properties of the xNi-2Al supports and the Pd/xNi-2Al catalysts determined by XRD and XPS measurements

x	Crystal size (nm)[a]				Theoretical atomic composition[b]	Surface atomic composition[c]
	xNi-2Al		Pd/xNi-2Al		Pd/xNi-2Al	Pd/xNi-2Al
	$NiAl_2O_4$ (2θ=37.0°)	NiO (2θ=43.3°)	$NiAl_2O_4$ (2θ=37.0°)	NiO (2θ=43.3°)	Al/Ni	Al/Ni
0.8	6.9	-	7.3	-	2.5	2.2
0.9	7.9	-	8.1	-	2.2	1.9
1.0	7.8	6.6	7.8	6.6	2	1.7
1.1	8.2	6.4	8.2	6.8	1.8	1.6

[a]The crystal sizes of $NiAl_2O_4$ and NiO were calculated by the Scherrer equation from the XRD peaks at 2θ=37.0° and 43.3°, respectively
[b]Theoretical compositions were calculated based on concentrations of precursor solutions
[c]Surface atomic compositions were determined by XPS measurements

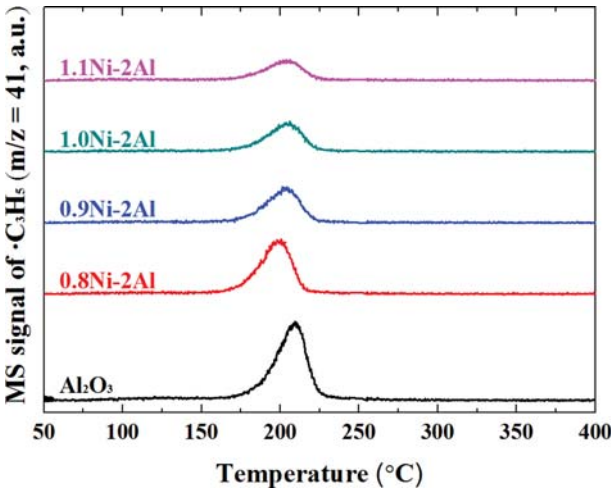

Fig. 2. IPA-TPD profiles of the xNi-2Al supports. The mass signal of *m/z*=41 (·C_3H_5) represents a fragment of the propylene radical produced from the dehydration of IPA.

the surface decreased progressively. This can be accounted for by the variation in content of unsaturated Al^{3+} ions in the supports upon increasing the Ni content. As unsaturated Al^{3+} ions act as Lewis acid centers in the spinel structure [39], a decrease in the quantity of exposed unsaturated Al^{3+} ions at the surface results in a decrease in the number of surface acidic sites upon increasing the Ni content. Although the evolved peak temperature of the xNi-2Al supports shifted slightly towards lower temperatures compared to Al_2O_3, no significant difference was observed amongst the different xNi-2Al supports.

4. XPS Analysis before Methane Combustion Reaction

Amongst the various factors affecting the catalytic activity of the methane combustion reaction, the chemical state of the Pd species (i.e., metallic Pd^0, PdO, and PdO_2) plays an important role [15, 20]. Thus, XPS measurements were performed to analyze the chemical states of the supported Pd species. Fig. 3(a) shows the Pd 3d XPS spectra of the Pd/xNi-2Al catalysts before the methane combustion reaction. Through peak deconvolution, the presence of different Pd species was confirmed, and the peak positions and relative atomic compositions are summarized in Table 3. More specifically, in the Pd $3d_{5/2}$ spectra, characteristic peaks corresponding to Pd^0, Pd^{2+}, and Pd^{4+} were observed at 335.2, 336.7, and 338.4 eV, respectively [15,20,25]. Although it is known that the bulk palladium

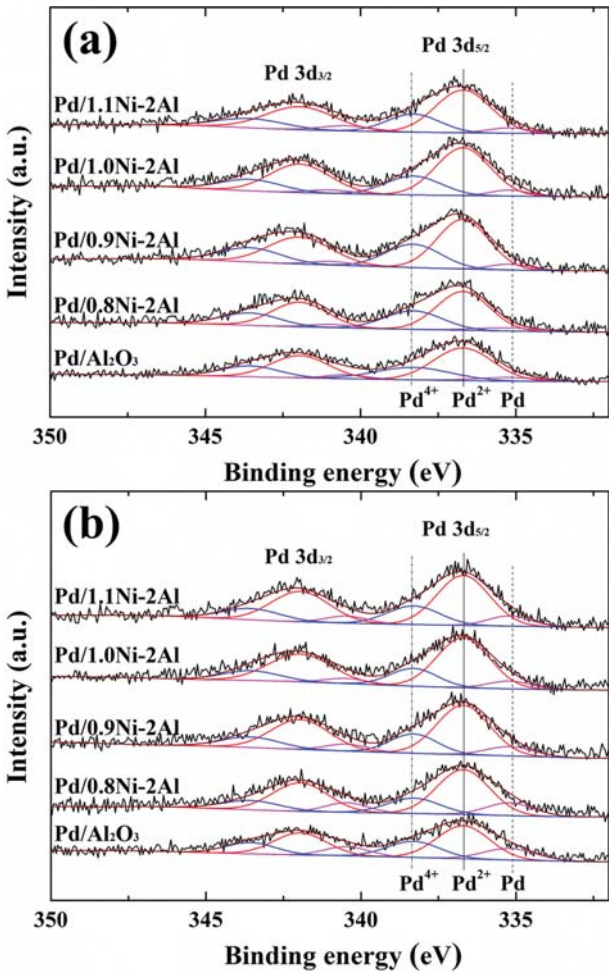

Fig. 3. Pd 3d XPS spectra of the Pd/xNi-2Al catalysts (a) before and (b) after the methane combustion reaction carried out at 370 °C for 20 h in the presence of 3% water vapor.

cannot exist in the form of PdO_2 at the temperatures above 200 °C [37], PdO_2 could be observed in the case of supported Pd catalysts even after calcination at relatively high temperatures [13,18]. As shown in Fig. 3(a) and Table 3, the Pd^{2+} composition exhibited a volcano-shaped curve, which varied in intensity based on the Ni content, with a maximum being observed for the Pd/1.0Ni-2Al catalyst. Although a number of studies [13,14] have reported that Pd^0 plays a major role in the adsorption and activation of methane,

Table 3. Electron binding energy and atomic composition obtained from the Pd $3d_{5/2}$ spectra of the Pd/xNi-2Al catalysts before and after the methane combustion reaction carried out at 370 °C for 20 h in the presence of 3% water vapor

x in Pd/xNi-2Al	Binding energy (eV) (Atomic composition, %)					
	Before reaction			After reaction		
	Pd^0	Pd^{2+}	Pd^{4+}	Pd^0	Pd^{2+}	Pd^{4+}
0	335.2 (7.8)	336.7 (61.8)	338.4 (30.4)	335.2 (19.0)	336.7 (54.5)	338.4 (26.5)
0.8	335.2 (6.4)	336.7 (61.3)	338.4 (32.3)	335.2 (16.1)	336.7 (62.5)	338.4 (21.4)
0.9	335.2 (5.7)	336.7 (62.6)	338.4 (31.7)	335.2 (11.1)	336.7 (65.8)	338.4 (23.1)
1.0	335.2 (6.0)	336.7 (67.0)	338.4 (27.0)	335.2 (8.9)	336.7 (69.0)	338.4 (22.1)
1.1	335.2 (6.5)	336.7 (66.7)	338.4 (26.8)	335.2 (10.8)	336.7 (65.0)	338.4 (24.2)

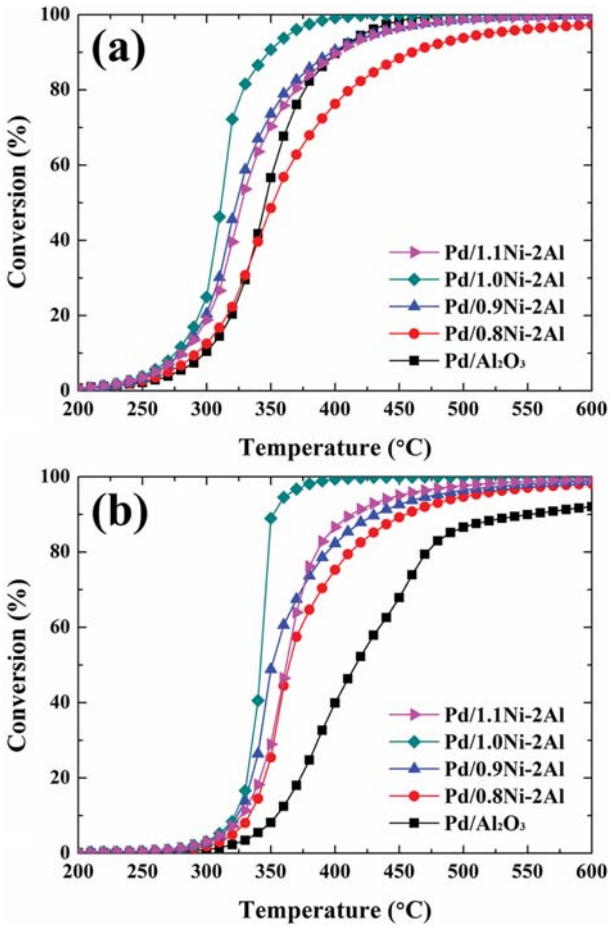

Fig. 4. Catalytic performance of the Pd/xNi-2Al catalysts in the methane combustion reaction as a function of reaction temperature in (a) the absence and (b) the presence of 3% water vapor.

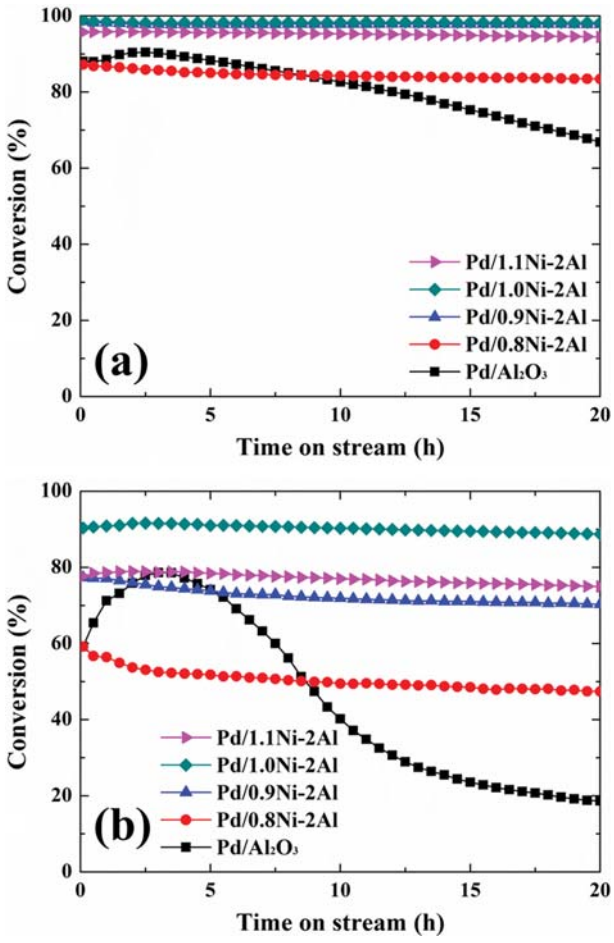

Fig. 5. Isothermal methane combustion reactions of the Pd/xNi-2Al catalysts carried out at 370 °C for 20 h in (a) the absence and (b) the presence of 3% water vapor.

it is generally accepted that a higher Pd^{2+} content results in a higher catalytic activity [2,3], and so the initial conversion of the Pd/1.0Ni-2Al catalyst is expected to exhibit the best catalytic performance amongst samples. This is because the Pd/1.0Ni-2Al catalyst initially possessed the highest Pd^{2+} composition (see Pd^{2+} atomic composition of the catalysts before reaction in Table 3), likely due to the support-metal interaction, which depends on the Ni content.

5. Catalytic Activity and Stability in Methane Combustion Reaction

Fig. 4 shows the results of the temperature-programmed methane combustion reactions carried out both in the presence and absence of 3% water vapor. In the absence of water (i.e., dry condi-

Table 4. Catalytic activity and stability of the Pd/xNi-2Al catalysts in the methane combustion reaction in the presence and absence of 3% water vapor

x in Pd/xNi-2Al	Temperature programmed						Isothermal				
	Dry (°C)			Wet (°C)			Dry (%)		Wet (%)		
	$T_{20\%}$ [a]	$T_{50\%}$ [a]	$T_{90\%}$ [a]	$T_{20\%}$ [a]	$T_{50\%}$ [a]	$T_{90\%}$ [a]	$X_{0.1\,h}$ [b]	$X_{20\,h}$ [b]	$X_{0.1\,h}$ [b]	$X_{20\,h}$ [b]	R_d [c]
0	321	346	401	373	414	550	88.0	66.8	59.2	18.6	68.6
0.8	316	351	460	345	364	456	87.2	83.4	59.2	47.4	20.0
0.9	301	325	400	334	352	430	98.6	97.8	77.4	70.3	9.2
1.0	294	312	350	331	342	351	99.0	98.3	90.4	88.8	1.8
1.1	301	327	401	341	362	411	95.7	94.5	77.7	75.0	3.5

[a]Temperature required to reach methane conversions of 20, 50, and 90%

[b]Conversion at 0.1 and 20 h

[c]Deactivation rates were calculated by $(X_{0.1\,h}-X_{20\,h})/X_{0.1\,h}$

tions, Fig. 4(a)), the Pd/1.0Ni-2Al catalyst exhibited the best performance, and the catalytic activities of the various Pd/xNi-2Al catalysts increased in following order: Pd/0.8Ni-2Al<Pd/Al_2O_3< 1.1Ni-2Al<Pd/0.9Ni-2Al<Pd/1.0Ni-2Al. Interestingly, in the presence of water (i.e., wet conditions, Fig. 4(b)), the Pd/1.0Ni-2Al catalyst again exhibited the highest catalytic activity; however, all samples (and in particular Pd/Al_2O_3) showed reduced catalytic activities under wet conditions, as outlined in Table 4. This is likely due to the water vapor acting as an inhibitor towards methane combustion [11,23,27,28].

To confirm the stability of the as-prepared catalysts, isothermal reactions were carried out at 370 °C for 20 h in the presence and absence of 3% water vapor, as shown in Fig. 5 and Table 4. Under dry conditions, all catalysts exhibited high stability and conversions, with the exception of Al_2O_3 (Fig. 5(a)). In addition, the conversion of the isothermal reaction was somewhat higher than that obtained in the temperature-programmed reaction at 390 °C (see Fig. 4(a)). This is likely due to deactivation taking place during the temperature-programmed reaction upon increasing the temperature. As indicated in Fig. 5(b), in the presence of 3% water vapor, a significantly different trend was observed. In this case, the initial conversions exhibited volcano-shaped curve (see Table 4), and this tendency corresponded with the Pd^{2+} compositions of the fresh catalysts (i.e., Pd/0.8Ni-2Al≈Pd/Al_2O_3<Pd/0.9Ni-2Al<1.1Ni-2Al< Pd/1.0Ni-2Al), as confirmed by XPS measurements (Fig. 3(a)). In addition, the deactivation rates also varied as a function of the Ni content, and the Pd/Al_2O_3 catalyst underwent severe deactivation. More specifically, the catalyst deactivation rates represented volcano-shaped curve, depending on Ni content with the smallest value being observed for the Pd/1.0Ni-2Al catalyst, thereby indicating that the Pd/1.0Ni-2Al catalyst exhibited the highest conversion and hydrothermal stability of the various catalysts examined herein.

As discussed previously, although the 1.0Ni-2Al support was synthesized under stoichiometric conditions to produce the spinel $NiAl_2O_4$ structure, it also contained a small quantity of NiO on the surface. Thus, the possibility that the surface NiO species participating in the methane combustion reaction could not be excluded at this point. Although Zou et al. [24] reported that γ-Al_2O_3-supported NiO catalyst exhibited negligible activity up to 400 °C, Shen et al. [40] demonstrated that the presence of NiO can enhance the re-oxidation ability in the Mars and van Krevelen redox mechanism through the formation of a NiO-PdO alloy structure. More specifically, in the presence of water vapor, the oxygen migration from support to active site was inhibited by water molecules adsorbed; however, the presence of NiO adjacent to Pd species can support the re-oxidation of reduced Pd species. It is therefore possible that the excellent hydrothermal stability of the the Pd/1.0Ni-2Al catalyst could be partially attributed to the co-existence of both PdO and NiO [25].

6. XPS Study after Methane Combustion Reaction

To analyze the reason for the varying deactivation rates at different Ni contents, XPS analysis was performed on the samples following the isothermal reaction at 370 °C for 20 h in the presence of 3% water vapor, as shown in Fig. 3(b) and Table 3. To allow a clear comparison, the Pd^{2+} composition before and after the reactions is indicated in Fig. 6(a) along with the conversions after 20 h under wet conditions. As indicated, the atomic composition of Pd^{2+} varied significantly after the reaction, and consequently the conversion after 20 h corresponded with Pd^{2+} composition at this time. However, the changes in atomic composition after the isothermal reaction exhibited different trends depending on the Ni content. In contrast to the remainder of the samples, the Pd^{2+} composition decreased for the Pd/Al_2O_3 and Pd/1.1Ni-2Al catalysts. It is normally accepted that an increase in Pd^{2+} composition corresponds to an improvement in the methane combustion activity; however, in this case, deactivation was observed for all samples.

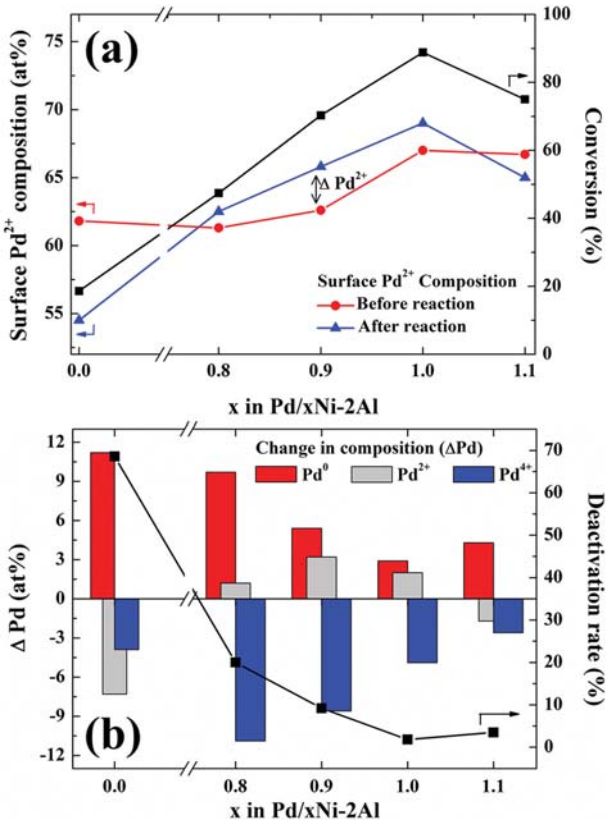

Fig. 6. (a) Correlation curves between the Pd^{2+} composition as determined by XPS analysis and the conversion after 20 h under wet conditions. (b) Changes in the atomic composition of the Pd species and corresponding deactivation rates of the Pd/xNi-2Al catalysts.

Based on the above observations, it is necessary to confirm not only the changes in Pd^{2+} composition, but also those of Pd^0 and Pd^{4+} during the reaction. As outlined in Fig. 6(b), the variation in the atomic compositions of the Pd species after the reaction is represented by ΔPd, and thus the changes in the Pd^0, Pd^{2+}, and Pd^{4+} compositions are denoted as ΔPd^0, ΔPd^{2+}, and ΔPd^{4+}, respectively. Although a number of studies suggest that Pd^0 is involved in the adsorption and activation of methane, both Pd^0 and Pd^{4+} are mainly considered to be inactive in the methane combustion reaction, while Pd^{2+} is considered to be the active species [9,10,15]. Compared to the fresh catalyst, ΔPd^{4+} decreased for all catalysts during the reaction, indicating that the metastable Pd^{4+} was reduced to Pd^{2+} or

metallic Pd^0 [41-43]. As a result, the deactivation rate correlated with ΔPd^0. For example, although the content of inactive Pd^{4+} decreased in the Pd/Al_2O_3 catalyst, the metallic Pd^0 content significantly increased, thereby resulting in severe deactivation. In contrast, a lesser degree of deactivation was observed for the Pd/1.0Ni-2Al catalyst, due to the relatively small increase in Pd^0 content. In addition, Zou et al. [24] and Liu et al. [23] reported that the support-metal interactions can be modified at the $NiAl_2O_4$ interface due to the impregnation of PdO by epitaxy formation, which leads to intimate contact and strong interaction between the support and impregnated PdO. Therefore, the changes in ΔPd as a function of Ni/Al ratio were likely due to variation in the support-metal interactions, which were dependent on the composition of the support.

7. Reducibility Test by CH_4-TPR

The reducibility of active sites has attracted great interest in the methane combustion reaction because this reaction is known to follow the Mars and van Krevelen reduction-oxidation pathway [14,24,40,44]. According to this mechanism, the first step involves reduction of the PdO species by methane, followed by a second step where Pd is re-oxidized by oxygen. Thus, the differences in shapes and temperatures of the TPR profiles may correlate with their catalytic performance [18,45,46]. In addition, the majority of studies have shown that TPR curves are sensitive to a number of factors, including the type of support, the active metal dispersion, and the presence of promoters. Fig. 7 shows the CH_4-TPR profiles of the Pd/xNi-2Al catalysts between 200 and 400 °C, where deconvolution into two major peaks, namely α and β, is observed. The α reduction peak had lower peak center compared to the β peak, meaning that the reducible species corresponding the α peak is more readily reduced than that of β peak. In the case of Pd/1.0Ni-2Al catalyst, which showed the best catalytic performance of the various catalysts examined, exhibited the lowest reduction peak temperature and the highest portion of crystalline PdO, as outlined in Table 5. It therefore indicated that the excellent catalytic activity of this catalyst can be partially attributed to the high reducibility of the PdO species. As discussed in the previous chapter, the co-existence of PdO and NiO can enhance the re-oxidation ability [40], resulting in good hydrothermal stability during the reaction under wet conditions. From the results of CH_4-TPR, it can be seen that the proper amount of NiO can also improve the reducibility of catalyst. Therefore, both activity and stability can be improved with the optimal content of surface NiO.

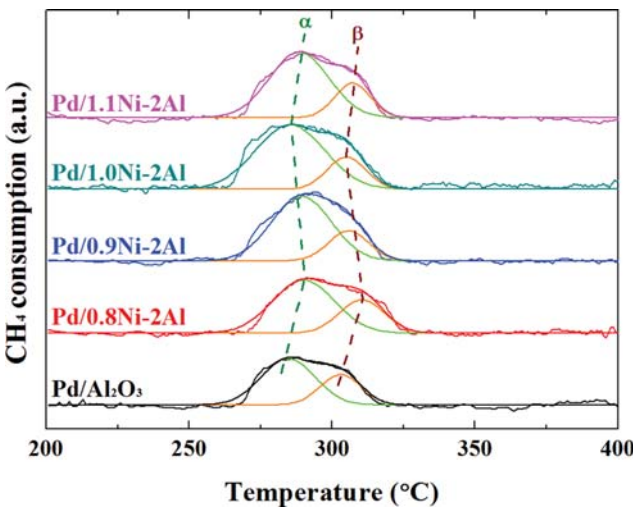

Fig. 7. Reduction behavior of the Pd/xNi-2Al catalysts as determined by CH_4-TPR measurements.

Table 5. Reduction temperatures and relative PdO content of the reduction peaks obtained from CH_4-TPR experiments

x in Pd/xNi-2Al	Reduction temperature (°C) (Relative portion, %)	
	α Peak	β Peak
0	284.6 (66.7)	303.1 (33.3)
0.8	290.1 (68.6)	310.5 (31.4)
0.9	289.3 (76.0)	305.8 (24.0)
1.0	283.6 (78.1)	303.6 (21.9)
1.1	288.5 (76.1)	307.2 (23.9)

CONCLUSIONS

We synthesized xNi-2Al oxide (x=0-1.1) supports via a hydrothermal method, followed by their subsequent application to the catalytic methane combustion reaction after the impregnation of Pd. It was found that the metal-support interactions were affected by the Ni content, and thus the catalytic activity and stability in the methane combustion reaction were also largely influenced by the Ni content. In addition, the catalytic activity correlated with the Pd^{2+} composition, and the stability corresponded with the change in Pd^0 content during the reaction.

Although the preparation of the 1.0Ni-2Al support under stoichiometric conditions produced the spinel structure $NiAl_2O_4$, determination of the surface atomic composition by XPS indicated that the surface contained small quantities of NiO. In addition, the Pd/1.0Ni-2Al catalyst exhibited optimal catalytic activity and stability of all examined catalysts both in the presence and absence of 3% water vapor. This is likely due to the Pd species on the 1.0Ni-2Al support maintaining a high Pd^{2+} ratio both before and after the reaction stages. Furthermore, it was confirmed that the Pd/1.0Ni-2Al catalyst contained the highest proportion of crystalline PdO species, which were more easily reduced than amorphous PdO.

ACKNOWLEDGEMENT

This research was supported by Basic Science Research Program through the National Research Foundation of Korea (NRF) funded by the Ministry of Science, ICT and Future Planning (2017R1A2B3011316).

SUPPORTING INFORMATION

Additional information as noted in the text. This information is available via the Internet at http://www.springer.com/chemistry/journal/11814.

REFERENCES

1. A. Bill, A. Wokaun, B. Eliasson, E. Killer and U. Kogelschatz, *Energy Convers. Manage.*, **38**, S415 (1997).
2. R. Hayes, *Chem. Eng. Sci.*, **59**, 4073 (2004).
3. J.-H. Park, J. H. Cho, Y. J. Kim, E. S. Kim, H. S. Han and C.-H. Shin, *Appl. Catal., B: Environ.*, **160-161**, 135 (2014).
4. A. Baylet, S. Royer, P. Marecot, J.-M. Tatibouet and D. Duprez, *Appl. Catal., B: Environ.*, **77**, 237 (2008).
5. L. Liotta, G. Di Carlo, G. Pantaleo and G. Deganello, *Catal. Commun.*, **6**, 329 (2005).
6. K. Huang, L. Wang, Y. Xu and D. Wu, *Korean J. Chem. Eng.*, **34**, 1366 (2017).
7. J. Li, R. Hu, J. Zhang, W. Meng, Y. Du, Y. Si and Z. Zhang, *Fuel*, **178**, 148 (2016).
8. Z. Pu, H. Zhou, Y. Zheng, W. Huang and X. Li, *Appl. Surf. Sci.*, **410**, 14 (2017).
9. K. Persson, A. Ersson, K. Jansson, N. Iverlund and S. Järås, *J. Catal.*, **231**, 139 (2005).
10. G. Pecchi, P. Reyes, R. Gómez, T. López and J. Fierro, *Appl. Catal., B: Environ.*, **17**, L7 (1998).
11. G. Diannan, W. Sheng, C. Zhang, Y. Zhongshan and W. Shudong, *Chinese J. Catal.*, **29**, 1221 (2008).
12. B. Yue, R. Zhou, Y. Wang and X. Zheng, *Appl. Surf. Sci.*, **252**, 5820 (2006).
13. L.-f. Yang, C.-k., Shi, X.-e. He and J.-x. Cai, *Appl. Catal., B: Environ.*, **38**, 117 (2002).
14. K.-i. Fujimoto, F. H. Ribeiro, M. Avalos-Borja and E. Iglesia, *J. Catal.*, **179**, 431 (1998).
15. D. Gao, C. Zhang, S. Wang, Z. Yuan and S. Wang, *Catal. Commun.*, **9**, 2583 (2008).
16. J. E. Park, B. B. Kim and E. D. Park, *Korean J. Chem. Eng.*, **32**, 2212 (2015).
17. W. Yang, D. Li, D. Xu and X. Wang, *J. Nat. Gas Chem.*, **18**, 458 (2009).
18. T. Takeguchi, S. Aoyama, J. Ueda, R. Kikuchi and K. Eguchi, *Top. Catal.*, **23**, 159 (2003).
19. T. Takeguchi, O. Takeoh, S. Aoyama, J. Ueda, R. Kikuchi and K. Eguchi, *Appl. Catal., A: Gen.*, **252**, 205 (2003).
20. F. Yin, S. Ji, P. Wu, F. Zhao and C. Li, *J. Catal.*, **257**, 108 (2008).
21. P. Marti, M. Maciejewski and A. Baiker, *Appl. Catal., B: Environ.*, **4**, 225 (1994).
22. N. Guilhaume and M. Primet, *J. Chem. Soc. - Farad. T.*, **90**, 1541 (1994).
23. Y. Liu, S. Wang, T. Sun, D. Gao, C. Zhang and S. Wang, *Appl. Catal., B: Environ.*, **119-120**, 321 (2012).
24. X. Zou, Z. Rui, S. Song and H. Ji, *J. Catal.*, **338**, 192 (2016).
25. X. Pan, Y. Zhang, Z. Miao and X. Yang, *J. Energy Chem.*, **22**, 610 (2013).
26. H. Widjaja, K. Sekizawa, K. Eguchi and H. Arai, *Catal. Today*, **47**, 95 (1999).
27. M. A. Hoque and K. Kim, *Korean J. Chem. Eng.*, **31**(8), 1316 (2014).
28. R. Burch, F. Urbano and P. Loader, *Appl. Catal., A: Gen.*, **123**, 173 (1995).
29. A. Boumaza, L. Favaro, J. Lédion, G. Sattonnay, J. Brubach, P. Berthet, A. Huntz, P. Roy and R. Tétot, *J. Solid State Chem.*, **182**, 1171 (2009).
30. Y. H. Kim and E. D. Park, *Appl. Catal., B: Environ.*, **96**, 41 (2010).
31. G. Busca, *Catal. Today*, **226**, 2 (2014).
32. S. Rane, Ø. Borg, J. Yang, E. Rytter and A. Holmen, *Appl. Catal., A: Gen.*, **388**, 160 (2010).
33. B. Rebours, J. -B. d'Espinose de la Caillerie and O. Clause, *J. Am. Chem. Soc.*, **116**, 1707 (1994).
34. J. Zhang, H. Xu, X. Jin, Q. Ge and W. Li, *Appl. Catal., A: Gen.*, **290**, 87 (2005).
35. B. Vos, E. Poels and A. Bliek, *J. Catal.*, **198**, 77 (2001).
36. E. Hong, H.-I. Sim and C.-H. Shin, *Chem. Eng. J.*, **292**, 156 (2016).
37. E. Hong, S. W. Baek, M. Shin, Y.-W. Suh and C.-H. Shin, *J. Ind. Eng. Chem.*, **54**, 137 (2017).
38. S. Pyen, E. Hong, M. Shin, Y.-W. Suh and C.-H. Shin, *Mol. Catal.*, **448**, 71 (2018).
39. C. O. Areán, M. P. Mentruit, A. L. López and J. Parra, *Colloids Surf., A*, **180**, 253 (2001).
40. J. Shen, R. E. Hayes, X. Wu and N. Semagina, *ACS Catal.*, **5**, 2916 (2015).
41. K. Otto and L. Haack, *Appl. Catal., B: Environ.*, **1**, 1 (1992).
42. J. G. McCarty, *Catal. Today*, **26**, 283 (1995).
43. L. Borkó, I. Nagy, Z. Schay and L. Guczi, *Appl. Catal., A: Gen.*, **147**, 95 (1996).
44. C. A. Müller, M. Maciejewski, R. A. Koeppel and A. Baiker, *Catal. Today*, **47**, 245 (1999).
45. P. Castellazzi, G. Groppi, P. Forzatti, A. Baylet, P. Marécot and D. Duprez, *Catal. Today*, **155**, 18 (2010).
46. C.-k. Shi, L.-f. Yang, Z.-c. Wang, X.-e. He, J.-x. Cai, G. Li and X.-s. Wang, *Appl. Catal., A: Gen.*, **243**, 379 (2003).

Supporting Information

Methane combustion over Pd/Ni-Al oxide catalysts: Effect of Ni/Al ratio in the Ni-Al oxide support

Eunpyo Hong*, Su-A Jeon*, Sang-Sup Lee, and Chae-Ho Shin*,†**

*Department of Chemical Engineering, Chungbuk National University, Chungbuk 28644, Korea
**Department of Environmental Engineering, Chungbuk National University, Chungbuk 28644, Korea
(*Received 8 April 2018 • accepted 27 May 2018*)

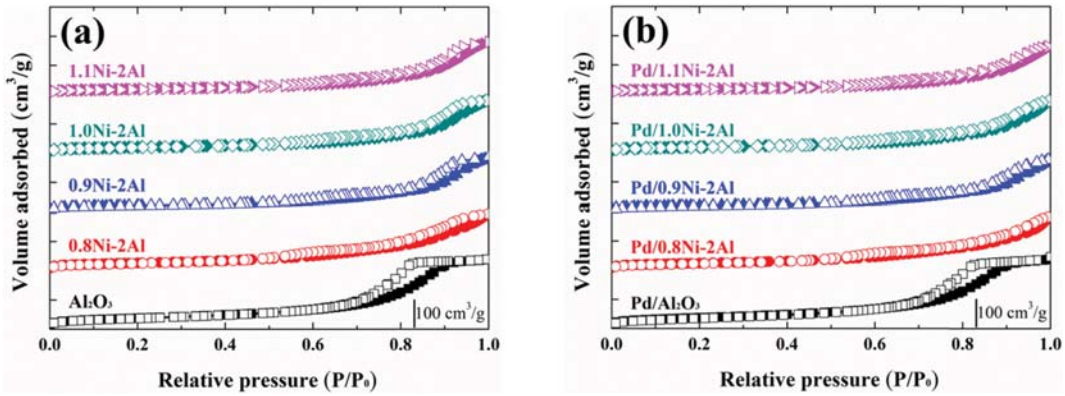

Fig. S1. N_2-sorption isotherms of (a) the xNi-2Al supports, and (b) the Pd/xNi-2Al catalysts.